Jurnal Kejuruteraan 37(3) 2025: 1387-1396
https://doi.org/10.17576/jkukm-2025-37(3)-23

Stereometric Analysis of Underfilled Micro Ball Grid Array Solder Joints Under Thermal Cycling Conditions

Muhammad Firdaus Suhaimi[a], Maria Abu Bakar[a*], Azman Jalar[a,b], Adlil Aizat Ismail[a,c], Muhammad Nizam Ilias[a,c], Mohamad Riduwan Ramli[d], Fakhrozi Che Ani[c] & A. Atiqah[a]

[a]*Institute of Microengineering and Nanoelectronics,*

[b]*Department of Applied Physics, Faculty of Science and Technology,*

Universiti Kebangsaan Malaysia, 43600 Bangi, Selangor, Malaysia

[c] *SanDisk Storage Malaysia Sdn. Bhd.*

Plot 301A, Persiaran Cassia Selatan 1, Taman Perindustrian Batu Kawan,

MK13, Batu Kawan, Seberang Perai Selatan, 14100, Penang, Malaysia

[d]*School of Materials and Mineral Resources Engineering, Engineering Campus,*

Universiti Sains Malaysia, 14300, Nibong Tebal, Pulau Pinang.

[*]*Corresponding author: maria@ukm.edu.my*

Received 22 November 2023, Received in revised form 5 October 2024
Accepted 5 November 2024, Available online 30 May 2025

ABSTRACT

Micro ball grid array (BGA) technology has gained attention due to the increasing density and miniaturization of BGA packages. Underfill is applied to BGA components to protect solder joints from mechanical and thermal stress, and reducing the risk of solder joint failure during thermal cycling test (TCT). Numerous studies have explored underfill materials, processing, and dispensing patterns in BGA components, but less focus on quantitative impact of underfills towards solder joint damage. This study employs stereometric analysis to quantify underfill-induced damage on micro-BGA solder joints after TCT. Micro BGA components on PCBs were compared with underfill (Sample A) and without underfill (Sample B). Each TCT involved four samples from A and B, subjected to same TCT conditions for 500, 750, and 1000 cycles. After each TCT cycle, all samples were analyzed using X-ray imaging, while three underwent dye and pull (DNP) testing and one was prepared for cross-sectional microstructural observation using an optical microscope. ImageJ software was used for stereometric analysis of solder joints post-DNP testing, focusing on coverages solder area. After 1000 TCT cycles, three cracks were identified in Sample B at the corners of the solder joint. The coverage area of solder joints with underfill (Sample A) was 30% higher than those without. The results indicate that underfill applications effectively prevent solder joint damage, as no cracks were observed in the micro BGA solder joints with underfill, highlighting its role in enhancing solder joint reliability.

Keywords: Micro ball grid array; crack occurrence; stereometric analysis; thermal cycling test; underfill application

INTRODUCTION

The development and advancement of electronic products and applications has been driven by rapid advancements in technology, resulting in increased miniaturization, improved functionality, and better performance. These advancements not only facilitate the rise of consumer electronics for telecommunication, such as smartphones and wearable devices, but also boost emerging applications in healthcare, automotive, and Internet of Things (IoT) (Muhammad et al. 2023; Sahar et al. 2024; Sampe et al. 2023; Yeap et al. 2024; Zailah et al. 2024).

Ball Grid Array (BGA) is the leading technology in surface mount devices (SMD) to connect the electronic components onto a Printed Circuit Board (PCB). BGA was introduced in 1990 and since then has dominated as a preferable technology in manufacturing electronic devices (Inoue et al. 2011). The BGA technology also dominates with equivalent of surface mount technology (SMT) such as Pin Grid Array (PGA) in terms of superior density, enhanced performance with shorter leads and exceptional conduction of heat (Jung et al. 2020) It was reported that BGA technology possesses superior electrical performance due to a shorter path from substrate to printed circuit board (PCB) (Liji et al. 2002; Jones et al. 2021). As the electronic packaging technology rapidly develop, the usage of micro BGA is established to serve the miniaturization, high density, smaller, lower cost, enhanced heat conduction and lighter weight of the electronic devices (Abas et al. 2016; Nashrudin et al. 2020). A standard BGA is typically 0.8 mm to 1.00 mm of ball pitch. Meanwhile, micro BGA has a ball pitch of 0.5 mm or less (Stoyanov et al. 2020). Thus, this enables smaller BGA packages which lead to overall miniaturization of electronic devices.

Similar to conventional BGA, micro BGA also face challenges on the reliability (Wen & Shen, 2021). Therefore, underfills were also introduced in the micro BGA packages to enhance the strength. Underfills have been widely used in BGA component to provide good structural integrity to the BGA component in terms of eliminating crack occurrence under thermal, mechanical stress, mechanical shock, and for reliability of the BGA package (Ismail et al. 2022a). Many attempts have been made to understand the underfills application such as underfills processing such as the flow of the underfills during dispensing and curing (Nashrudin et al. 2021) underfills materials properties and behavior (Lall et al. 2022; Kim et al. 2023), underfill underfilling methodology such as dispensing pattern, volume and etc. (Hung et al. 2024). Although the underfills application in BGA has been established, there are some missing parts on the damages effect of the BGA solder joint about applying the underfills. This is shown by previous reports that has investigated the underfill application on BGA via modelling study (Nashrudin et al. 2021; Tung et al. 2021). From the report, there are still on-going research work regarding applying the underfill onto BGA packages which showing some research gap on damages that could occurred between the application of underfill and BGA, for example, effect on dispensing pattern of underfill to BGA package. Therefore, the importance of designing the optimum underfill application on BGA package is for minimizing the damages of the solder joint, reduced the cost of applying underfills for good coverage of underfills that could protect the solder joint.

In order to understand the reliability of the BGA package with underfill applications, thermal cycling test (TCT) is used to determine the reliability of the solder joint. TCT is a reliability test which exposes the samples with cyclic range of temperature. The TCT can determine the strength of component to withhold the thermal stress during the cyclic temperature (Kim et al. 2023). TCT can determine the component ability to resist extremely low and extremely high temperatures, as well as their ability to withstand cyclical temperatures exposure (Jiang et al. 2019). One of the common issues of BGA solder joint is the solder balls experiences large shear stress due to the large difference in the value of Coefficient of Thermal Expansion (CTE) between the silicon die and the PCB which resulted in failure of the solder ball in form of cracking. This failure was attributed to the fatigue failure of the solder ball particularly during the cyclic thermal exposure during TCT which created thermomechanical stress (Shi et al. 2018). Therefore, this works aimed to investigate the underfills application on BGA packages subjected to TCT testing from 500, 750 and 1000 cycles by analyzing the quantitative coverage of underfills via stereometric analysis. The stereometric analysis will help the electronic packaging industry in designing the underfill applications by estimating the qualitative and quantitative of underfill coverage to the BGA solder joint. The outcome of this work will give some understanding of the damage that could have occurred without the underfill application.

MATERIALS AND METHOD

Two types of samples were used in this study: a micro BGA package with underfill application (namely sample A) a micro BGA package without underfill application (namely B), which serve as the control. Lead-free solder paste, Sn-3.0Ag-0.5Cu (SAC305) with type 5 with solder particles ranged of 15-25 μm was used to connect the BGA packages onto the printed circuit board (PCB) substrate with

dimensions of 200 mm length × 200 mm width × 0.8 mm thickness. Each micro BGA package consists of 48 solder balls as shown in Figure 1. The micro BGA packages were soldered on the PCB via reflow soldering process with maximum temperature of 235 °C in the reflow oven (BTU). To prepare sample A, an underfill material of amount 1.5 mg was dispensed to the micro BGA component on the PCB. Figure 2 illustrated the top view of solder ball arrangement in micro BGA package and direction of the underfill dispensed to the micro BGA package. The underfill was dispensed using automated mode using a bespoke DJ-9500 (NORDSON). The underfill was jetted at a 2 mm dispense gap relative to PCB using a commercial grade epoxy material. The properties of the underfill are shown in Table 1. After dispensing, the whole micro BGA package of sample A was cured in a HCZ Vertical Curing Oven with temperatures ranging from 140 °C to 180 °C for 20 minutes.

A1	B1	C1	D1	E1	F1	G1	H1
A2	B2	C2	D2	E2	F2	G2	H2
A3	B3	C3	D3	E3	F3	G3	H3
A4	B4	C4	D4	E4	F4	G4	H4
A5	B5	C5	D5	E5	F5	G5	H5
A6	B6	C6	D6	E6	F6	G6	H6

FIGURE 1. Illustration of solder balls arrangement for the micro BGA package

TABLE 1. Underfill properties

Underfill properties	Value
Filler maximum size range	20 µm
Viscosity	4 Pa.s
Tg	120°C
CTE 1 (Below Tg)	35 ppm/°C
CTE 2 (After Tg)	156 ppm/°C
Curing condition	160°C for 6 min
Floor life	48 hours

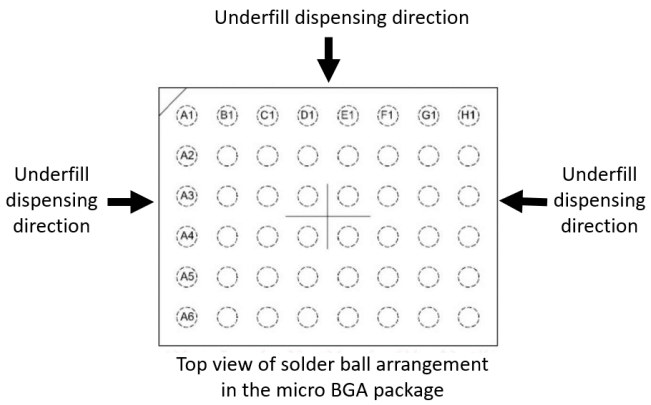

FIGURE 2. Illustration of top view of solder ball arrangement in micro BGA package and direction of the underfill dispensed to the micro BGA package.

For reliability testing, sample A and sample B were subjected to TCT for 500, 750, and 1000 cycles, in accordance with the JESD22-A104 standard. In each TCT, four samples of both Sample A and Sample B were tested, resulting in a total of 192 solder joints for each test. The samples were subjected to TCT under temperature ranges from -40°C to 85°C, with a temperature change rate of 0.16°C/s and dwell time of 600 seconds. After each TCT cycle, comprehensive characterizations testing was carried out on all four micro BGA that consists of 192 solder joints. X-ray (GE Phoenix Micromex 180) inspection is used to detect any abnormalities or internal defects in the solder joints in terms of shape and size.

Then, three out of four micro BGA package were then undergo dye and pull (DNP) test to assess the solder joint structural integrity. DNP testing was used to identify the crack location of the solder ball matrix array and is widely utilized for reliability testing (Cruz et al. 2022; Ismail et al. 2022b). DNP involves cleaning the sample to remove the debris and the flux around the solder, then putting it on a red dye by immersion. To ensure the dye penetrates all cracks, the samples were then exposed to vacuum environment. The samples were then baked at 70 °C for 3 hours in an oven. To avoid smearing, the ink must be fully dried. Then, the micro BGA package is separated by the PCB's prying at the edges of the component. The separated interfaces of the pried component were observed using optical microscope.

Next, the dye penetration area on the solder ball was measured using ImageJ software. Subsequently, for stereometric analysis, the images were analyzed using ImageJ software and converted to 8-bit (black and white) format. The scale of the images was calibrated according to the scale provided by the optical microscope. Figure 3 shows the example of steps conducted to calculate the solder ball area using ImageJ software. Using ImageJ, the raw image from the optical microscope was converted to 8-bit format, the white color threshold image was changed to red, and the area outline was drawn manually to calculate the solder ball area. Figure 4 illustrates the steps for using ImageJ software to calculate the dye-penetrated area. Figure 4(a) shows an example of a solder joint with dye penetration, which will be zoomed in to display the single solder joint and Figure (b) shows a yellow line sketch outlining the perimeter of the dye-penetrated region, with the area calculated based on this sketch.

For microstructural observations, one samples of A and B were prepared into a cross-sectional via metallographic technique including samples cutting, cold mounting, grinding and polishing process. The last row (A6-H6) of the solder ball array for each sample was targeted for microstructural analysis and comparison. Sample A and B were laser cut perpendicularly relative to the micro BGA package and PCB. Then, the samples were transferred in a 30 mm diameter of round shaped molds. Next, the mixture of epoxy resin and hardener flowed into the molds and kept at room temperature for 24 hours until it hardened completely. Both samples were grinding with Silicon Carbide paper of 240, 320, 600, 800, 1000 and 2000 grit sizes with flowing water. After that, the polishing process was executed using diamond paste of 6, 3 and 1 micron followed by oxide polishing for up to 60 seconds (Ismail et al. 2021; Jalar et al. 2020).

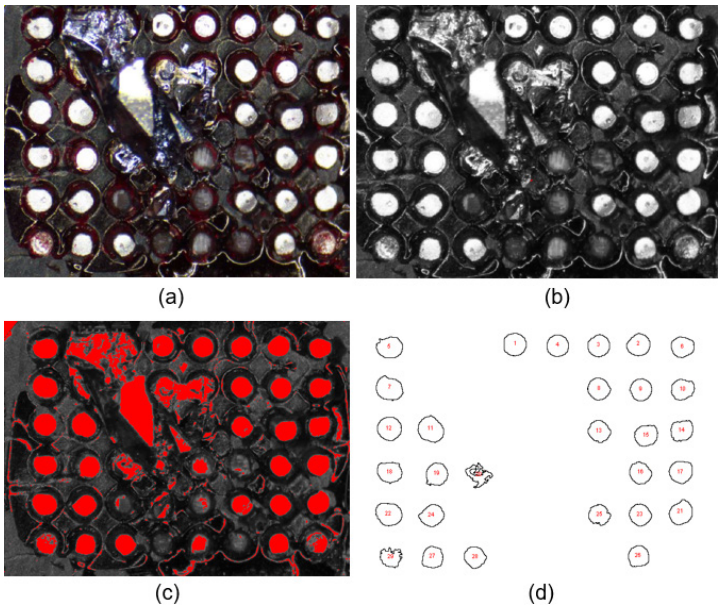

FIGURE 3. Example of steps using ImageJ software to calculate the solder ball area: (a) Example of raw image of top view solder balls taken using optical microscope (b) Example of an image that has been converted into 8 bits using ImageJ (c) Example of white color threshold has been changed into red color (d) Example of bare outline of the red area for solder ball area calculation.

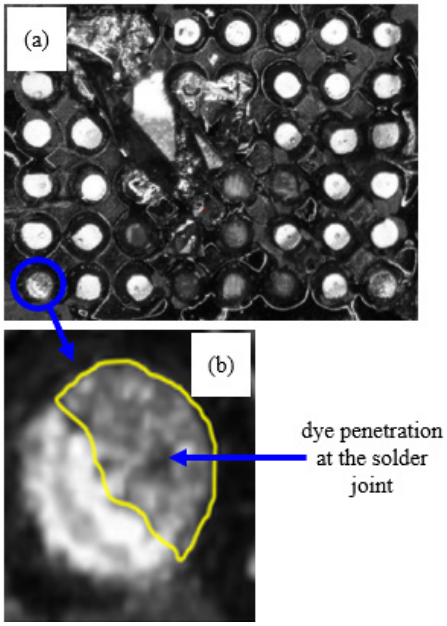

FIGURE 4. Example of steps of using ImageJ software to calculate the dye penetrated area of the solder ball: (a) Example of top-view image solder ball with dye penetration. This image with dye penetration will be zoomed in as a single image showing a single solder ball and (b) Top view image of solder ball with a yellow line sketch was created to outline the perimeter area of the dye-penetrated region, and the area was calculated based on the sketch.

RESULTS AND DISCUSSION

After 500, 750 and 1000 cycles of TCT, all samples A and B were characterized using X-ray to observe any abnormalities that could have occurred on the micro BGA solder joint. The Xray results show that there are no abnormalities such as solder bridging, irregular solder ball size found for all samples A and B after 500, 750 and 1000 cycles of TCT. Figure 5 shows an example of X-ray images for sample A and B after 1000 cycles of TCT. Both samples exhibit no visible cracks in the images (Figure 5). The average diameter of the micro BGA from the Xray image is 320 µm for sample A and 315 µm sample B. The results indicate that the solder ball diameters are similar in both conditions (with and without underfill).

Table 2 shows the micro BGA components and solder ball quantity affected by the dye penetration subjected to TCT. For all entries under Sample A, there were zero components affected. In contrast, Sample B demonstrated that one out of three micro BGA components was affected after 1000 cycles. Additionally, 3 out of 48 solder joints in Sample B were affected after the same number of cycles. Cross-sectional analysis revealed that Sample B exhibited cracks in 3 out of 48 solder joints. Consequently, Sample A reported a failure rate of 0%, while Sample B showed a failure rate of 6%.

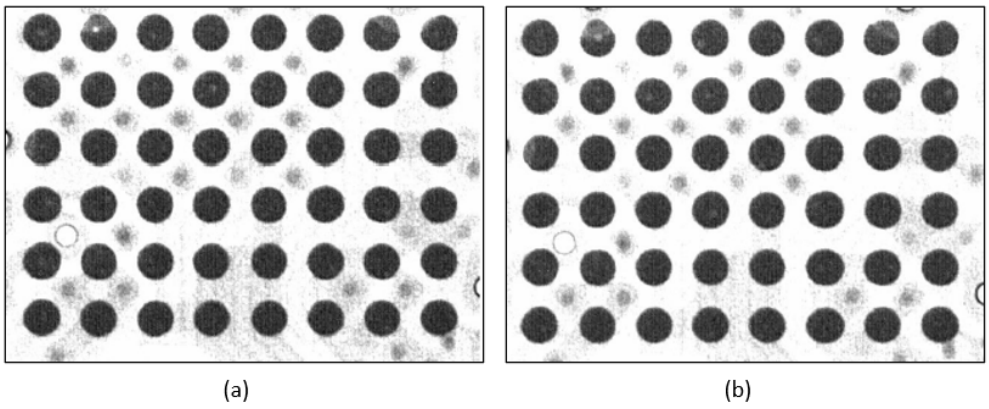

FIGURE 5. Example of X-ray images for: (a) Sample A and (b) Sample B after TCT for 1000 cycles

TABLE 2. Micro BGA component and solder ball quantity affected by the dye penetration subjected to the thermal cycling tests.

Sample	Sample quantity	Thermal cycling test (cycle)	Component quantity affected by the dye penetration	Solder joint affected by the dye penetration	Solder joint crack via cross section analysis	Solder joint failure
A	4	500	0	0	0	0
A	4	750	0	0	0	0
A	4	1000	0	0	0	0
B	4	500	0	0	0	0
B	4	750	0	0	0	0
B	4	1000	1/3	3/48	3/48	6%

Figure 6 shows an example of DNP images of both sample A and B. Dye penetration was observed exclusively in Sample B, which did not have underfill, while no dye penetration was detected in Sample A post TCT for 1000 cycles. It was found that dye penetration occurred at the edge location of solder joint on each side which are ball A6 G6 and H6 as shown in Figure 6(d) and 6(f) respectively. The dye penetration area for A6 and H6 are 55% and 78% respectively. Lesser dye penetration of 15% was observed for G6 Figure 6(f). The shape of the dye penetration is like half-moon for A6 and crescent shaped for H6 ball. From this observation, it clearly seen that the dye penetration initiated from the edge (H6) of the solder joint and propagated centripetally toward the center (G6).

From the DNP images, a quantitative analysis via stereometric approach has been used to measure the coverage of solder joint area as shown in Figure 7 and 8, respectively. It is shown that more coverage of solder joint for sample A with underfill application can be obtained as compared to sample B. The solder joint area coverage for sample A is slightly uniform with range of 6.0 to 6.7 $\mu m^2 \times 10^4$ as compared to sample B with range of 4.0 to 5.7 $\mu m^2 \times 10^4$. The result shows that the coverage area will underfill applications approximately, 30% higher as compared to those without underfill application. This shows that underfill applications contribute to better solder joint reliability after TCT at 1000 hours.

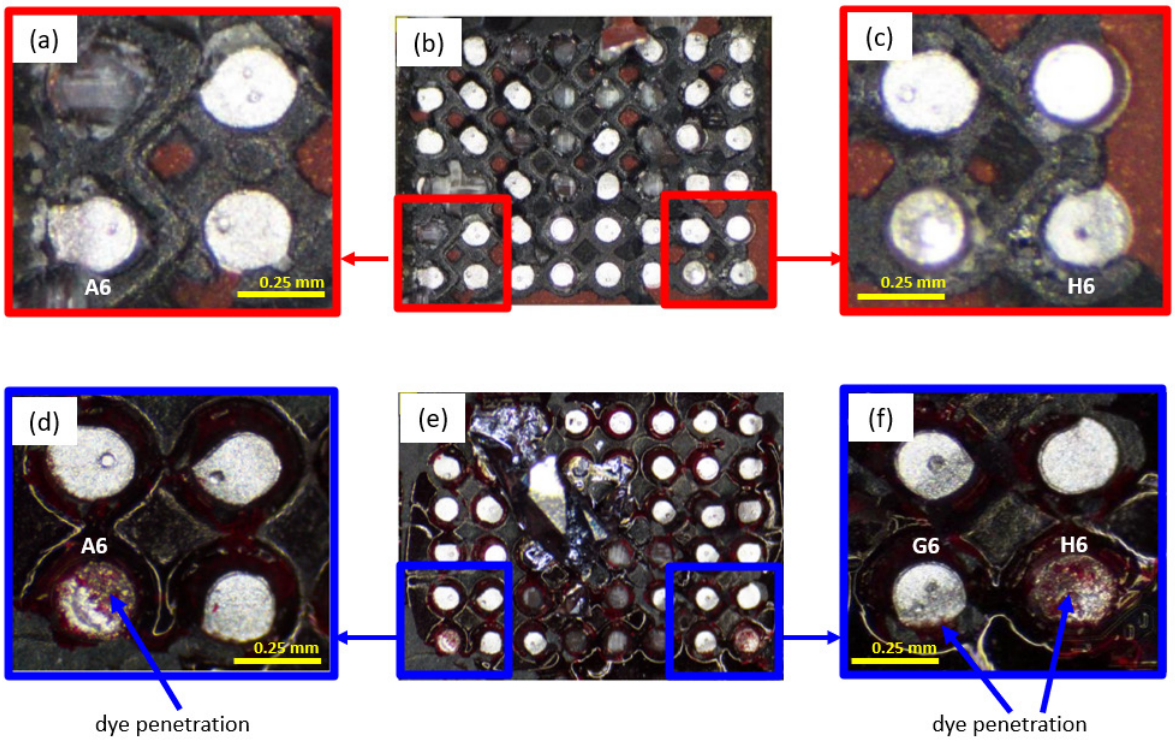

FIGURE 6. Example of micrographs solder balls from the micro BGA post-Dye and Pull (DNP) test. Sample A shows no dye penetration in (a), (b), and (d), while dye penetration is clearly observed in Sample B (c) at positions A6 (d), G6 (e), and H6 (f) after 1000 thermal cycling test (TCT) cycles.

FIGURE 7. Example of solder joint area for sample A after DNP test for 1000 cycles

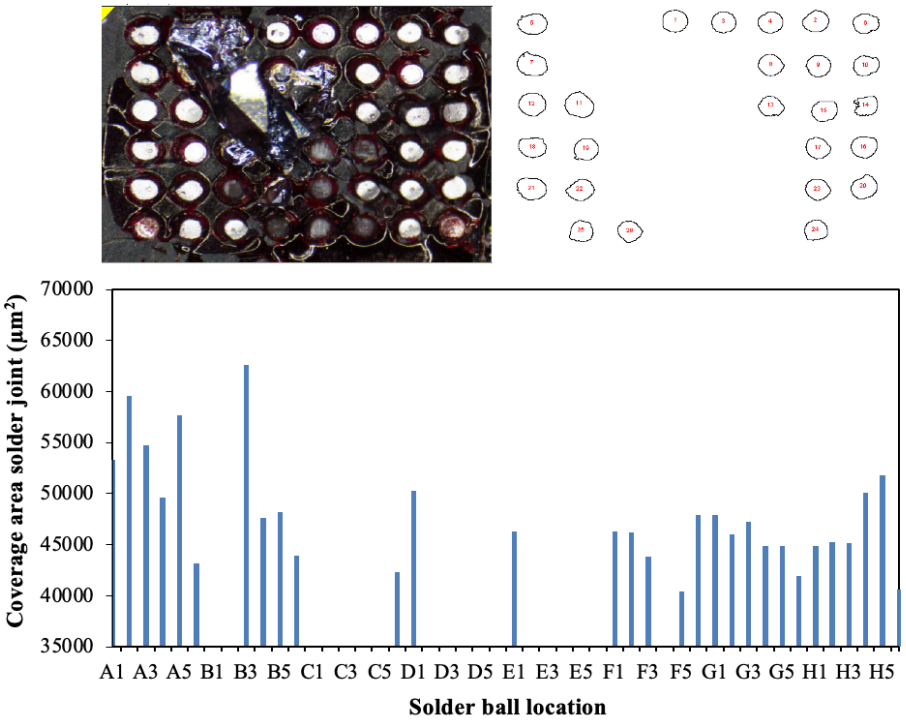

FIGURE 8. Example of solder joint area for sample B after DNP test for 1000 cycles.

Figure 9 shows micrographs of cross-sectional solder joints for sample A and B after 1000 cycles of TCT. Based on the figure, there is no crack occurred in sample A while sample B exhibits clear crack occurrence at locations of A6 (Figure 9 (e)), G6 (Figure 9 (g)) and H6 (Figure 9 (h)). The crack length at the solder joint of sample B located at position A6 with 312 µm crack line along the solder joint. This significant crack highlights the level of the structural damage observed after 1000 cycles, indicating the solder joint failure. Solder joint with position B6 shows fewer signs of solder joint damage, with voids visible near the top, but no clear cracks. For solder joint with position G6 shows similarity to sample B A6 whereby the cracks and voids are visible along the top edge of the solder joint. Shorter crack line of A6 (Figure 9 (g)) is approximately 48 µm. Multiple cracks are observed across the top of the solder joint for sample B with position H6, indicating severe degradation, along with voids that could potentially weaken the joint further. The crack line of sample B H6 is 221 µm, shorter than at A6.

This result is in line with the DNP in Figure 6 which showing the cracks of sample B with position A6, G6 and

H6 are prone to be formed at the corner location of solder ball array. The crack initiated at the edge of the solder joint, where the stress concentration is typically higher, thus, leading to the formation of crack under TCT condition. This result confirms the findings from DNP test where there is no dye penetration in underfilled sample, which indicate that underfill able to enhance the strength of the solder ball during the TCT test.

The results show that without underfill application, the solder joint is prone to have crack occurrences. Furthermore, the crack occurrence is contributed by CTE mismatch between the component and the PCB. During TCT test, the solder balls between the component and PCB undergo cyclic thermal stress. This cyclic stress eventually resulted in the thermal fatigue of the solder joint which caused it to form cracks in the bulk of the solder joint. It is shown that the crack initiated at the top right side of the solder ball and move through the bulk solder from right to left. However, crack in sample B at H6 initiated from the left to the right side of the bulk solder. Since the cross section was done in the Z plane of the solder ball, the crack initiation point may bias towards any crack that occurred near the plane. It can be said that the difference in crack origin is insignificant due to the cross-section method. Nevertheless, it is seen that the crack initiated from the edge of the solder ball and propagated centripetally towards its center.

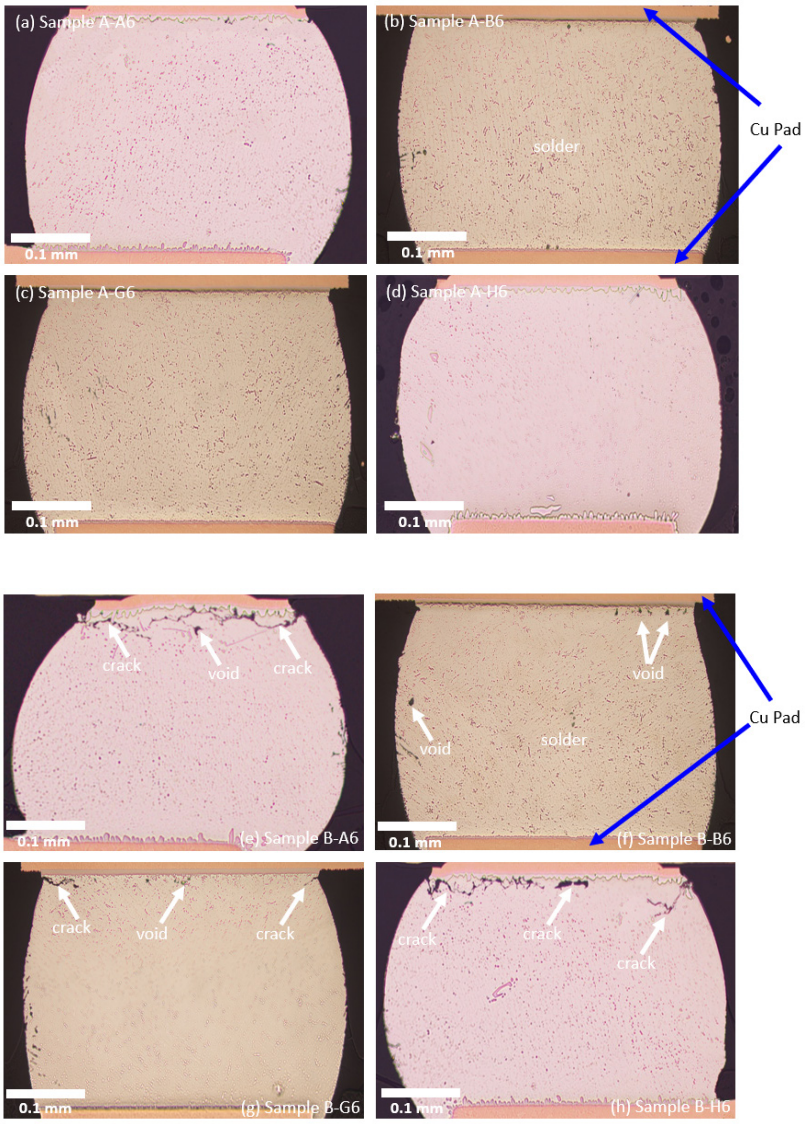

FIGURE 9. Solder joint cross-sectional micrographs for sample A at locations: (a) A6, (b) B6, (c) G6 and (d) H6, and for sample B at locations: (e) A6, (f) B6, (g) G6 and (h) H6 after 1000 cycles of TCT.

CONCLUSION

This study successfully investigated the impact of underfill application on the solder joints of micro BGAs subjected to thermal cycling tests (TCT). The results indicated that one out of three micro BGAs without underfill (sample B) exhibited vulnerability, with some components and solder joints showing dye penetration after 1000 cycles. Cross-sectional analysis revealed that 3 out of 48 solder balls experienced crack occurrences, primarily at the edges of the micro BGA, resulting in approximately 6% solder joint failure. The cracks were observed to form and propagate from the edge of the solder joint toward the center. In contrast, the findings indicate that micro BGAs with underfill demonstrate high reliability, exhibiting no signs of dye penetration, solder joint cracks, or failures throughout all TCT. This demonstrates that underfill applications effectively eliminate damages associated with crack occurrences.

ACKNOWLEDGEMENT

The authors would like to acknowledge the financial support provided by Universiti Kebangsaan Malaysia (research grant: GUP-2024-055) and SanDisk Storage Malaysia Sdn. Bhd (research grant: RR-2023-007) through our collaboration activities.

DECLARATION OF COMPETING INTEREST

None

REFERENCES

Abas, A., Haslinda, M.S., Ishak, M.H.H., Nurfatin, A.S., Abdullah, M.Z. & Ani, F.C. 2016. Effect of ILU dispensing types for different solder bump arrangements on CUF encapsulation process, *Microelectron. Eng.* 163: 83–97.

Cruz, R.S.V. & Gonda, V. 2022. Creep and Reliability Prediction of a Fan-Out WLP Influenced by the Visco-Plastic Properties of the Solder, *Acta Polytech. Hungarica*. 19: 236-254.

Hung, H.H., Cheng, Y.C., Hwang, S.J., Chang, H.J., Huang, B.Y., Huang, H.H., Chen, D.L., Wang, C.C. & Hung, C.P. 2024. Effect of flip-chip ball grid array structure on capillary underfill flow. *Results in Engineering* 23: 102527.

Inoue, A. 2011. Recent development and application products of bulk glassy alloys, *Acta Mater*. 59 (2011) 2243–2267.

Ismail, A.A., Bakar, M.A., Ehsan, A.A., Jalar, A., Ani, F.C. & Zolkefli, Z.E. 2022a. Effects of Underfill Materials on Behavior of Intermetallic Compound Thickness of Ball Grid Array Solder Joints Using ANOVA, in: *2022 IEEE 39th Int. Electron. Manuf. Technol. Conf., IEEE*: 1–5.

Ismail, A.A., Bakar, M.A., Ehsan, A.A., Jalar, A., Basiron, E. & Ani, F.C. 2022b. Cardinal and Ordinal Directions Approach in Investigating Arrayed Solder Joints Crack Propagation of Ball Grid Array Semiconductor Packages, *IEEE Trans. Components, Packag. Manuf. Technol.* 12: 1492–1501.

Ismail, N., Jalar, A., Bakar, M.A., Safee, N.S., Wan Yusoff, W.Y. & Ismail, A. 2021. Microstructural evolution and micromechanical properties of SAC305/CNT/CU solder joint under blast wave condition, *Solder. Surf. Mt. Technol.* 33: 47–56.

Jalar, A., Bakar, M.A. & Ismail, R. 2020. Temperature Dependence of Elastic–Plastic Properties of Fine-Pitch SAC 0307 Solder Joint Using Nanoindentation Approach, *Metall. Mater. Trans. A Phys. Metall. Mater. Sci. 51*: 1221–1228.

Jiang, N., Zhang, L., Liu, Z.Q., Sun, L., Long, W.M., He, P., Xiong, M.Y. & Zhao, M. 2019. Reliability issues of lead-free solder joints in electronic devices. *Science and Technology of Advanced Materials*. 20(1): 876–901.

Jones, R., Lang, J., Papyan, V., Peng, D., Lua, J. & Ang, A. 2021. Characterising crack growth in commercially pure titanium, *Eng. Fail. Anal.* 122: 105287.

Jung, D.A.E.Y., Cain, S.R. & Chen, W.T. 2020. Introduction to Wire Bond Technology, in: Encycl. Packag. Mater. Process. Mech. *Set 1 Interconnect Wafer Bond. Technol. Vol. 2 Wire Bond. Technol., World Scientific*, 2: 1–21.

Kim, D., Park, J., Jang, J., Yang, H., Kim, K., Oh, C. & Kim, D. 2023. Underfill material property dependence of lifetime and mechanical behavior of BGA package: EBSD and FEM investigations. *Microelectronics Reliability*. 150: 115113.

Kim, J. & Yoon, D. 2023. Thermomechanical Reliabilities of Pb-Free Solder Joints According to Ag Content in Harsh Environment, *IEEE Trans. Reliab*: 1-9.

Lall, P., Kasturi, M., Wu, H., Suhling, J. & Davis, E. 2022. Microstructural Evolution of Viscoelastic Properties of Underfills Under Sustained High Temperature Operation, *J. Electron. Packag.* 144.

Liji, Z., Li, W., Xiaoming, X. & Kempe, W. 2002. An investigation on thermal reliability of underfilled PBGA solder joints, *IEEE Trans. Electron. Packag. Manuf.* 25: 284–288.

Muhamad, N.A., Zahid, F.S., Othman, N. & Sin, N.D.M. 2023. The Role of IoT Technologies in Malaysia

During the Covid-19 Pandemic: A MiniReview. *Jurnal Kejuruteraan* 35(3): 587-595.

Nashrudin, M.N., Abas, A., Abdullah, M.Z., Ali, M. & Samsudin, Z. 2021. Study of different dispensing patterns of No-flow underfill using numerical and experimental methods, *J. Electron. Packag.* 143.

Nashrudin, M.N., Gan, Z.L., Abas, A., Ishak, M.H.H., Ali, M.Y.T. 2020. Effect of hourglass shape solder joints on underfill encapsulation process: numerical and experimental studies, Solder. *Surf. Mt. Technol.* 32: 147–156.

Sahar, N.M., Islam, M.T., Misran, N. & Ariffin, N.H. 2024. Litar Setara Dwi Jalur Antena Dwikutub Bersepadu untuk Aplikasi RFID. *Jurnal Kejuruteraan* 36(2): 641–651.

Sampe, J., Yunus, N.H.M., Yunas, J. & Ismail, A.G. 2023. Rekabentuk dan Prestasi Antena MEMS Penuai Tenaga Mikro Frekuensi Radio Bagi Peranti Elektronik Berkuasa Rendah. *Jurnal Kejuruteraan* 35(2): 265-273.

Shi, L., Chen, L., Zhang, D.W., Liu, E., Liu, Q. & Chen, C.-I. 2018. Improvement of thermo-mechanical reliability of wafer-level chip scale packaging, *J. Electron. Packag.* 140: 11002.

Stoyanov, S., Bailey, C., Stewart, P. & Morrison, G. 2020. Reliability impact of assembly materials for Micro-BGA components in high reliability applications, in: *2020 IEEE 8th Electron. Syst. Technol. Conf., IEEE* : 1–7.

Tung, L.H., Ng, F.C., Abas, A., Abdullah, M.Z., Samsudin, Z. & Tura Ali, M.Y. 2021. Effect of different temperature distribution on multi-stack BGA package, *Microelectron. Int.* 38: 33–45.

Wen, J. & Shen, J. 2021. Solution to engineering problems of silicon-optical switches: reliability of co-package, in: AOPC 2021 Micro-Optics MOEMS, SPIE: 104–119.

Yeap, K.H., Ng, L.L., Mazlan, A.U., Loh, S.H. & Tshai, K.H. 2024. Dynamic Power Saving for CMOS Circuits. *Jurnal Kejuruteraan* 36(4): 1399–1407.

Zailah, W., Gan, B.Y.J., Leong, H.Y., Sahar, N.M. &Islam. T.A. 2022. Vision-based Inspection of PCB Soldering Defects. *Jurnal Kejuruteraan* 34(5): 807-817.